Journal of Applied Polymer Science

Experimental study on the penetration interfaces of pipes with different cross-sections in overflow water-assisted coinjection molding

Tang-Qing Kuang,[1] Kai Zhou,[1] Li-Xuan Wu,[2] Guo-Fa Zhou,[3] Lih-Sheng Turng[4]

[1]Department of Material Science and Engineering, School of Mechanical and Electrical Engineering, East China Jiaotong University, Nanchang 330013, China

[2]Technology Development Center for Polymer Processing Engineering of Guangdong Province, Guangdong Industry Technical College, Guangzhou 510300, China

[3]School of Environmental and Chemical Engineering, Nanchang University, Nanchang 330000, China

[4]Polymer Engineering Center and Wisconsin Institute for Discovery, University of Wisconsin-Madison, Madison, Wisconsin 53706

Correspondence to: L.-S. Turng (E-mail: turng@engr.wisc.edu)

ABSTRACT: The residual wall thicknesses (RWT) of the skin and the inner layers are important quality indicators of water-assisted coinjection molding (WACIM) parts. The influences of the shape of the cavity cross section and the processing parameters, including the water pressure, water delay time, inner melt temperature, and inner melt flow rate, on the penetration of the inner melt and water were explored via experiments. The results showed that the shape of the penetration section of the inner melt was closer to the cavity section with round corners, while that of the water ended up being round. Both the penetration ratios of the inner melt and the water increased proportionally with increasing circle ratio. Both the minimum values of the total RWT and the inner melt RWT increased with increasing circle ratio. Both the maximum values of the total RWT and the inner melt RWT increased with increasing Max_D, which is the maximum distance between the inscribed circle center and the wall. Both the penetration ratios of the inner melt and the water increased with increasing water pressure, decreased with increasing water delay time, and increased with increasing inner melt flow rate and increasing inner melt temperature. © 2015 Wiley Periodicals, Inc. J. Appl. Polym. Sci. **2016**, *133*, 42866.

KEYWORDS: manufacturing; molding; thermoplastics

Received 1 June 2015; accepted 24 August 2015

DOI: 10.1002/app.42866

INTRODUCTION

Water-assisted coinjection molding (WACIM), an innovative processing technology used to manufacture hollow plastic parts with a multilayer structure, was first developed in Germany in 2004.[1,2] WACIM can be considered a combined processing technology of the water-assisted injection molding (WAIM) and coinjection molding (CIM) processes. It can be categorized into two types: short-shot WACIM (S-WACIM) and overflow WACIM (O-WACIM). In the S-WACIM process, the mold cavity is partially filled with two different polymer melts that are injected sequentially and form a skin/core structure, followed by the injection of water into the core of the polymer melt. In the O-WACIM process, the mold cavity is first completely filled with polymer melt, followed by high pressure water that pushes the materials into an overflow cavity.

WACIM has the advantages of WAIM and CIM, such as fast cooling, a smooth inner surface, thinner RWT, material savings, weight reduction, cost savings,[3,4] and comprehensive performance of different materials.[5] Moreover, it offers a wide processing window.[2] The first WACIM part, an engine cooling pipe with a diameter of 35 mm, was demonstrated at the 2004 K show in Dusseldorf, Germany. The 30% glass-filled nylon 66 was used as the external skin material to achieve mechanical strength and temperature resistance. The inner wall surface was made out of polypropylene, which offers a perfect channel surface quality and ideal media resistance.[1,2] WACIM technology is mainly used for automotive parts, household items, furniture, sports equipment, and children's toys, highlighting a bright future for WACIM with regard to market prospects.

Few groups have investigated the WACIM process. The Institute of Plastics Processing (IKV) at RWTH Aachen University studied and developed various fluid-assisted injection molding processes, including the WACIM process. Some scholars in East China Jiaotong University and Nanchang University in China have studied the WACIM process. Zhang *et al.*[6–8] studied the influence of water pressure, water flow rate, and water delay time on the penetration of the inner melt and water during the O-WACIM process in a circular pipe by numerical simulation. Kuang *et al.*[9] investigated the effects of the rheological properties of materials and the

Table I. Properties of the High-Density Polyethylene Used in the Experiments

Property	Measure	Value
Tensile yield stress	Q/SY DS 0512	30.4 MPa
Tensile break stress	Q/SY DS 0512	26.3 MPa
Density	Q/SY DS 0510	0.9566 g cm^2
Melt flow index	Q/SY DS 0511	7.3 g·(10 min)$^{-1}$
Impact strength	GB/1043.1-2008	5.8 kJ m^{-2}

processing parameters on the penetration of the inner melt and the water during the S-WACIM process in a circular pipe by numerical simulation. Yan[10] studied the influence of processing parameters on the temperature and velocity field during the filling stage of the O-WACIM process of a pipe with a square cross-section by numerical simulation. Cao[11] investigated the interface fluctuation in WACIM via numerical simulation. Zhou *et al.*[12] studied the effect of the inner melt temperature on the penetration behavior of the inner melt and the water in the WACIM process using the finite element method. Most of the studies mentioned above were limited to WACIM pipes with circular or square cross-sections. Zhou *et al.*[13] investigated the RWT of WAIM parts with noncircular cross-sections using the computational fluid dynamics (CFD) method. Kuang *et al.*[14] studied the influence of the cross-section on the penetration of the water in the O-WAIM process via experimentation. Kuang *et al.*[15] investigated the effect of the cross-section on the temperature field and the penetration sections of the inner melt and the water during the filling stage of O-WACIM via numerical simulation. However, to the best knowledge of the authors, there have been no reports of the systematical experimentation study of the penetration interfaces in the O-WACIM process in pipes with different cross-sections.

This research is devoted to studying the effects of cavity cross-section and the processing parameters on the penetration of the inner melt and the water in the O-WACIM process via experimentation. This study mainly includes the following. (1) Studying the effect of cross-section shape on the shape of the penetration sections and penetration ratios of the inner melt and the water and the total RWT and RWT of the inner melt. (2) Studying the effect of the processing parameters on the penetration ratios of the inner melt and the water. It was found that the shape of the cavity cross-section had a great impact on the penetration section of the inner melt, and less effect on that of the water. Both the penetration ratios of the inner melt and the water increased proportionally with increasing circle ratio. The total RWT and the inner melt RWT were dominated by the shape of the cavity cross-section. It was also found that both the penetration ratios of the inner melt and the water increased with increasing water pressure, inner melt flow rate, and inner melt temperature, and decreased with increasing water delay time.

EXPERIMENTATION

Materials

Polyethylene and polypropylene were used in the WACIM experiment for their appli cability in the WAIM process and the compatibility between them. High-density polyethylene (HDPE, Grade DMDA-8008, Dushanzi Petro chemical Co., China) and polypropylene (PP, Grade 1102K, Jinxi Petrochemical Co., China) were purchased and their characteristics are listed in Tables I and II, respectively.

Selden[16] and Li *et al.*[17] found that the viscosity ratio of the core melt to the skin melt had a great effect on the material distribution in the CIM process. They also found that a high viscosity ratio led to an uneven material distribution. Kuang[9] and Deng *et al.*[18] got the same result in their numerical simulation and experimentation of WACIM pipes with circular cross-sections. In order to get a stable penetration of the inner melt in the skin polymer, the HDPE material with the higher melt flow index (MFI) and the PP with the relatively lower MFI were used as the outer and inner materials, respectively. To conveniently identify the interface between the skin layer and the inner layer, black, and red colorants were added.

Equipment Setup

The experiments were carried out on a lab-developed WACIM experimental platform, which was comprised of a co-injection molding machine, a water injection unit, a mold with changeable inserts, and a control unit. The molding machine was a 110-ton coinjection molding machine (FB-110C, FCS Group, Taiwan). The lab-developed water-injection unit included a plunger water pump with a maximum pressure of 20 MPa, a pressure-regulating valve, a water tank, and a water injection pin. The switching of the water injection pin was accomplished via a pneumatic control system. The mold, which is shown in Figure 1, was able to accommodate inter changeable inserts to allow for flexibility in specimen geometry. An overflow pin, which was used to disconnect the part cavity and the overflow cavity, was located at the overflow channel and controlled by the pneumatic control system as well. In O-FACIM, the pin was drawn back during the water injection such that the melt could be pushed into the overflow cavity.

Geometry of the Cross-Sections of the Cavities

The main products of WACIM are pipes and beams. Five typical cross-section cavities with the same inscribed circle radius of 10 mm were chosen in this study and these sections are shown in Figure 2.The lengths of these cavities were 200 mm. All edges of the cavity were filleted with a 2-mm radius. The cross-section of A had no concave corners, while B had two concave corners, C and D had four concave corners, and E had six concave corners and two convex corners.

Table II. Properties of the Polypropylene Used in the Experiments

Property	Measure	Value
Yield strength	ASTM D-638	52.0 MPa
Bending modulus	ASTM D-790	2850 MPa
Hardness	ASTM D-785	112 R
Heat distortion temp.	ASTM D-648	364 K
Melt flow index	ASTM D-1238	20 g·(10 min)$^{-1}$
Impact strength	ASTM D-256	185 J m^{-1}

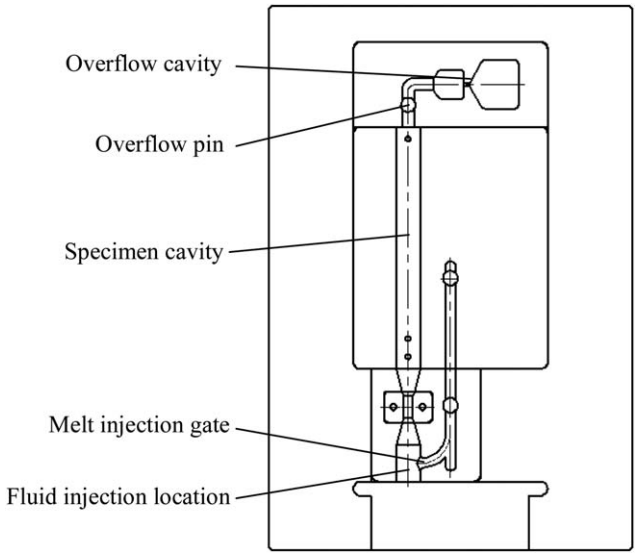

Figure 1. Diagram of the mold used in the experiments.

In order to conveniently compare and analyze the cavities, a circle ratio was introduced to characterize the sections.[13] A circle has a maximum circle radio of 1. Thus, the formula for calculating the circle ratio, α, was

$$\alpha = \frac{4\pi S}{C^2} \times 100\% \quad (1)$$

Where S denotes the area of the cross-section, and C denotes the circumference of the cross-section.

Geometric data for these sections, such as the area of the cross-section (A_{CS}), the maximum distance between the inscribed circle center and the wall (Max_D), and the circle ratio α, were calculated and are listed in Table III. Cavity A had the minimum Max_D, while cavities B and C had the same Max_D, and cavities D and E had the same Max_D. From cavities A to E,

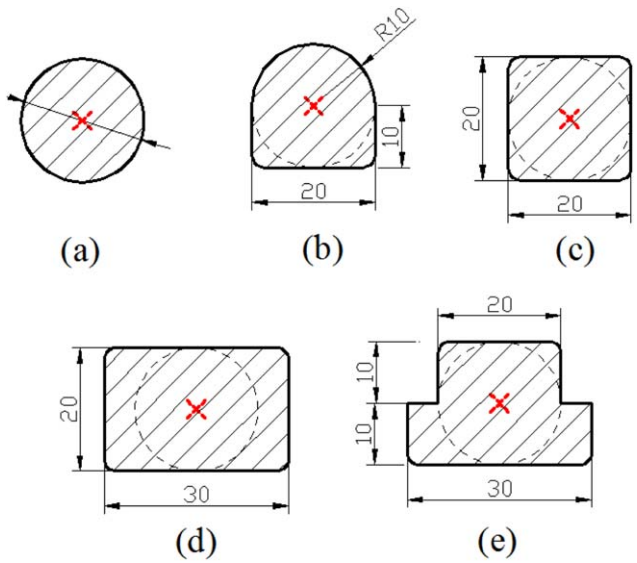

Figure 2. Cavity cross-sections used in the experiments. [Color figure can be viewed in the online issue, which is available at wileyonlinelibrary.com.]

Table III. Geometric Data of the Cross-Sections

Cross-Section No.	A_{CS} (mm^2)	Max_D(mm)	Circle Ratio α
(a)	314	10.00	100.0%
(b)	357	13.31	88.0%
(c)	397	13.31	78.5%
(d)	597	17.22	75.4%
(e)	497	17.22	62.8%

the circle ratios decreased one by one, while cavities C and D had similar circle ratios.

Method of Molding Process

It was found that the water penetration during S-WAIM can be divided into primary penetration and secondary penetration, while the primary penetration can be further divided into front segment and rare segment. The change of the penetration condition of water at different segments led to an obvious RWT decrease along the flow direction. And the short-shot size had a great effect on the RWT along the flow direction.[19,10] The penetration of the water in the O-WAIM process was relatively stable, which resulted in an even RWT in the flow direction. The present research focused on the O-WACIM process. An O-WACIM pipe of circular cross-section is shown in Figure 3. As can be seen, the RWTs of the skin layer and the inner layer were even in the flow direction. The thickness change at the end of the cavity resulted from the sharp change of cross-section before and after the end of the cavity. This could be improved by smoothing the transition between the end of cavity and the overflow channel.

Processing Parameters

In order to investigate the influence of the cross-section and processing parameters on the penetration interfaces of the inner melt and the water, basic processing parameters were set and are listed in Table IV. The WACIM process on a pipe with different cross-sections was performed using the processing parameters set.

It was found in the research[4,20–25] of the WAIM process of circular cross-section pipes that the main factors determining the RWT were the water pressure and the water delay time, besides the shot size of the melt. In the research of the CIM process,[16] it was found that the main factors determining the material distribution were the inner melt flow rate, the inner melt

Figure 3. Overflow WACIM specimen. [Color figure can be viewed in the online issue, which is available at wileyonlinelibrary.com.]

Table IV. Basic Processing Parameters

Processing parameters	Value
Outer layer melt temperature	483 K (210°C)
Inner layer melt temperature	483 K (210°C)
Water delay time	3 s
Water temperature	298 K (25°C)
Water pressure	6 MPa
Injection flow rate of outer melt	9.26 cm^3/s
Injection flow rate of inner melt	9.26 cm^3/s
Packing time	60 s

temperature, and the shot size. Therefore, four factors—the water pressure, the water delay time, the inner melt flow rate, and the inner melt temperature—were investigated for the O-WACIM process in this study. In order to understand the effects of these factors on the penetration of the inner melt and the water, single factor experiments, in which one factor changed while the other factors were kept constant, were carried out.

Characterization of Molded Parts

All of the specimens were cut into cross-sections at the midpoint of the length of the specimens. The penetration interfaces of the inner melt and water were characterized at this position. The penetration ratio was introduced to characterize the relative penetration area and defined as the ratio of the penetration area to the total area. The penetration ratio of the inner melt R_I and the penetration ratio of the water R_W were calculated per the following formulas.

$$R_I = A_I / A_T \quad (2)$$

$$R_W = A_W / A_T \quad (3)$$

Where A_I denotes the area of the penetration of the inner melt, A_T denotes the area of the cross-section, and A_W denotes the area of the penetration of the water. The penetration areas of the inner melt and the water were irregular and could not be calculated directly. The penetration interfaces could be traced via CAD software and the penetration area could be obtained easily.

The minimum and maxi mum values of the total RWT and those of the RWT of the inner layer were measured and averaged from five specimens at the same processing parameters. For non-circular cross-sections, the minimal RWTs were measured at the tangent position of the inscribed circle to the cross-section; the maximal RWTs were measured in the direction of the center of the cross-section to the distal wall.

RESULTS AND DISCUSSION

Effect of the Cross-Section of the Cavity on the Penetration Sections of the Inner Melt and the Water

The experimental specimens, produced by O-FACIM under the same process ing parameters, were cut into cross-sections at the midpoint of the length of the samples, as shown in Figure 4. The penetration areas of the inner melt and water were calculated by CAD software and their penetration ratios were obtained by formulas (2) and (3), respectively. The maximum and minimum total RWT and those of the inner melt were measured. All results are listed in Table V.

As can be seen from Figure 4, for the circular pipe, both the penetration section of the inner melt and that of the water were circular in shape. For the non-circular pipes, the penetration sections of the inner melt were similar to the cavity cross-sections, except for the round corners, while the shapes of the water penetrations always tended to be round. This was the result from the features of the temperature field distribution at the cross-sections and the material properties of the melts and the water. It can be seen from the filling stage of the WACIM process of noncircular pipes[15] that the temperature contours near the wall were similar to the cavity cross-sections, while those near the convex and concave corners tended to be round. At the concave corner, the temperature contours moved inward for more efficient cooling due to the larger radius area, while the temperature contours at the convex corner moved outward to the corner for poorer cooling due to the smaller radius area. The core temperature was high and uniform. The viscosity of the inner melt was slightly lower than that of the skin melt. Thus the inner melt could penetrate the skin melt in a stable manner. Near the wall, a lower temperature led to a higher viscosity and a correspondingly higher flow resistance. Therefore, the penetration sections of the inner melt were similar to the temperature contours near the wall. The water temperature was much lower than that of the melt. A frozen membrane formed at the penetration front of the water at the instant contact occurred between the water and the melt. The frozen membrane encapsulating the water penetrated the core of the melt with uniform temperature. Due to the much lower viscosity of water, the penetration front of water tended to be spherical in shape. Consequently, the penetration section of the water tended to be round.

As can be seen from Figure 4, for the circular pipe, both the RWTs of the skin layer and the inner layer were rather even. For the noncircular pipes, the maximum total RWT and inner melt RWT always occurred at the wall farthest from the center of the cross-section. Meanwhile, the minimum RWT always occurred at the wall nearest the center of the geometry. For

Figure 4. Cross-section of specimens (Left to Right: specimen a-e). [Color figure can be viewed in the online issue, which is available at wileyonlinelibrary.com.]

Table V. The Penetration Ratios and Residual Wall Thicknesses of the Specimens

Cross-Section	Penetration Ratio(%)		RWT(mm)			
	Inner melt	Water	Min_T_RT	Min_I_RT	Max_T_RT	Max_I_RT
(a)	65.57	45.12	3.72	1.84	3.92	1.74
(b)	62.32	43.51	3.44	1.68	6.34	2.98
(c)	60.09	41.74	2.56	1.46	6.12	3.04
(d)	59.02	40.25	1.72	1.24	7.92	3.92
(e)	57.56	38.74	1.24	0.98	8.14	4.20

Max_T_RT and Max_I_RT denote the maximum total RWT and the maximum inner melt RWT, respectively. Min_T_RT and Min_I_RT denote the minimum total RWT and the minimum inner melt RWT, respectively.

cavities B and E (which had a larger lower half area), the minimum RWT occurred at the middle of the lower wall.

Based on the data listed in Tables III and V, the relationship between the penetration ratio and circle ratio can be obtained, as shown in Figure 5. As can be seen in Figure 5, the penetration ratios of the inner melt and the water increased proportionally with increasing circle ratios of the cross-section. The relationships between the penetration ratios of the inner melt, that of the water, and the circle ratio of the cross-section were fitted as formula (4) and (5), respectively.

$$R_I = 0.22\alpha + 43.12\% \quad (4)$$

$$R_W = 0.18\alpha + 27.33\%\text{v} \quad (5)$$

With the same radius of the inscribed circle, the lower circle ratio meant more or larger concave corners. The temperature of the skin melt at the concave corner dropped sharply due to the efficient cooling there. The skin melt at the concave corner was hard to be pushed out by the inner melt due to its higher viscous resistance. Therefore, the relative penetration area of the inner melt decreased and its penetration ratio decreased correspondingly. The penetration section of the water always tended to be round. Thus, the higher the circle ratio of the cavity cross-section, the higher the penetration ratio of the water. Meanwhile, a lower circle ratio meant a longer circumference for the same size area, which led to an increasing flow resistance from the wall. That was yet another reason for the decrease of penetration ratios of the inner melt and the water with a decreasing circle ratio of cavity cross-sections.

It can be observed from the specimen cross-sections that the minimal RWT occurred at the tangent position of the inscribed circle to the cross-section. Although all five of the cross-sections had the same radius of the inscribed circle, the minimum total RWT and inner melt RWT of these five cross-sections didn't stay constant. Both of them increased with increasing circle ratio, which can be seen from Figure 6.

It can be observed from the cross-sections of the specimens that the maximum RWT always occurred at the wall farthest from the center of the cross-section. The maximum values of the total RWT, and those of the RWT of the inner melt in O-FACIM, for cavities B and C (which had the same Max_D), and cavities D and E (which had the same Max_D), were very close. Thus, there was a very close relationship between the maximum RWT and the Max_D. Based on the data listed in Tables III and V, the relationships between the maximum values of the total RWT that of the RWT of the inner layer, and the Max_D can be obtained, as shown in Figure 7. Increasing the Max_D resulted in a near-linear increase in the maximum values of the total RWT as well as that of the inner melt of O-FACIM.

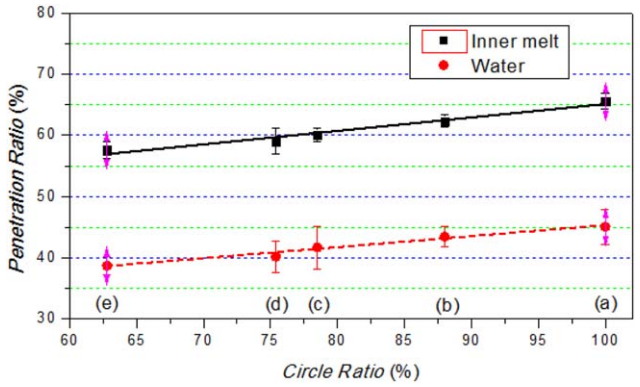

Figure 5. Penetration ratio as a function of circle ratio. (a-e are the no. of the cross-sections). [Color figure can be viewed in the online issue, which is available at wileyonlinelibrary.com.]

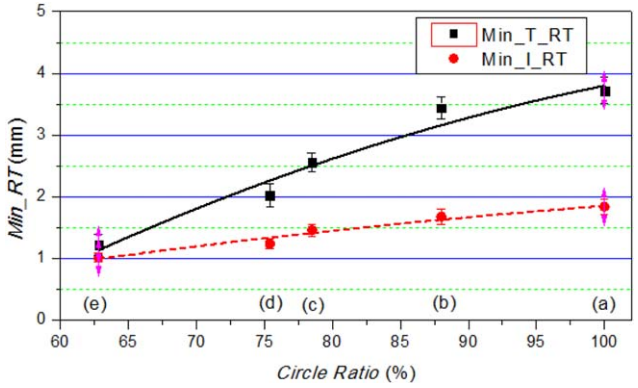

Figure 6. RWT as a function of circle ratio. (a-e are the no. of the cross-sections). [Color figure can be viewed in the online issue, which is available at wileyonlinelibrary.com.]

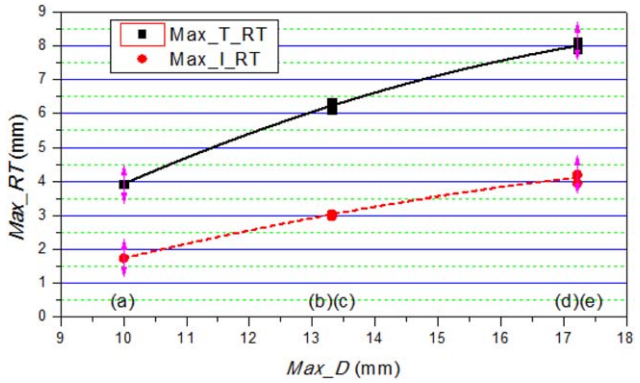

Figure 7. RWT as a function of distance between cavity wall and the center of its inscribed circle. (a-e are the no. of the cross-sections). [Color figure can be viewed in the online issue, which is available at wileyonlinelibrary.com.]

Effect of Processing Parameters on the Penetration Ratios of the Inner Melt and the Water

Effect of the Water Pressure on the Penetration Ratios of the Inner Melt and the Water. To investigate the influence of the water pressure on the penetration ratios of the inner melt and the water, the water pressure was set to 4, 6, 8, and 10 MPa, while keeping the other processing parameters constant. The penetration ratios of the inner melt and the water were calculated and are shown in Figure 8.

Figure 8 shows that the penetration ratios of the inner melt and the water increased with increasing water pressure. This was due to the fact that higher water pressure can push out more melt, which resulted in a larger penetration area of the water. The increase in water pressure led to a higher radial squeeze on the skin melt from the inner melt. Consequently, the penetration area of the inner melt increased.

Effect of the Water Delay Time on the Penetration Ratios of the Inner Melt and the Water. To investigate the influence of the water delay time on the penetration ratios of the inner melt and the water, the water delay time was set to 0, 3, 6, and 9 s, while keeping the other processing parameters constant. The penetration ratios of the inner melt and the water were calculated and are shown in Figure 9.

Figure 9 shows that the penetration ratios of the inner melt and the water decreased with increasing water delay time. This was due to the fact that the increase of the water delay time led to a greater decrease of the skin melt temperature, an increase in the thickness of the frozen layer, an increase in the viscosity of the melt, and an increase in the flow resistance, eventually resulting in a decrease of the inner melt penetration area. The increase of the overall penetration resistance led to a decrease in the water penetration area.

Effect of the Inner Melt Flow Rate on the Penetration Ratios of the Inner Melt and the Water. To investigate the influence of the inner melt flow rate on the penetration ratios of the inner melt and the water, the inner melt flow rate was set to 3.1 cm^3/s, 9.26 cm^3/s, 15.1 cm^3/s, and 21.7 cm^3/s, while keeping the other processing parameters constant. The penetration ratios of the inner melt and the water were calculated and are shown in Figure 10.

Figure 10 shows that the penetration ratio of the inner melt increased with increasing inner melt flow rate. This was due to the fact that the increased inner melt flow rate resulted from an increase of the injection pressure of the inner melt. A higher flow rate of the inner melt required a higher injection pressure. More skin melt could be pushed out by the inner melt, which resulted in an increased penetration area of the inner melt. The penetration resistance of the water decreased for the larger penetration area of the inner melt and the lower viscosity of the inner melt compared with that of the skin melt. Hence, more inner melt could be pushed out by the water and the water penetration area increased correspondingly.

Effect of the Inner Melt Temperature on the Penetration Ratios of the Inner Melt and the Water. To investigate the influence of the inner melt temperature on the penetration ratios of the inner melt and the water, the inner melt temperature was set to 200, 210, 220, and 230°C, while keeping the other processing parameters constant. The penetration ratios of the inner melt and the water were calculated and are shown in Figure 11.

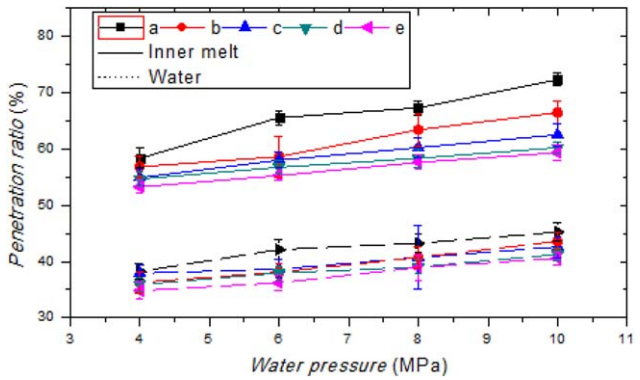

Figure 8. Penetration ratio as a function of water pressure. (a-e are the no. of the cross-sections). [Color figure can be viewed in the online issue, which is available at wileyonlinelibrary.com.]

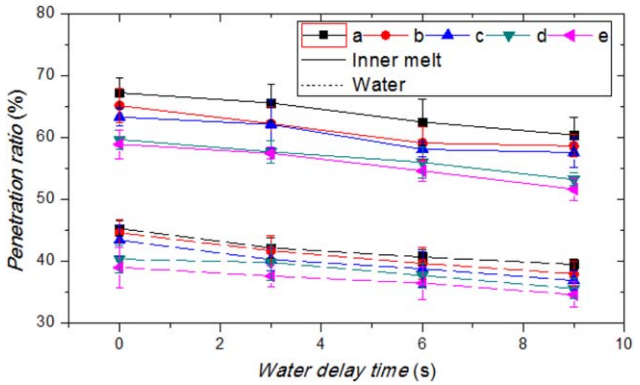

Figure 9. Penetration ratio as a function of water delay time. (a-e are the no. of the cross-sections). [Color figure can be viewed in the online issue, which is available at wileyonlinelibrary.com.]

Figure 11 shows that the penetration ratios of the inner melt and the water increased with increasing inner melt temperature. This was due to the fact that the inner melt viscosity and its flow resistance decreased with increasing inner melt temperature. The inner melt can push out more skin melt at the same pressure loss. Consequently, the penetration ratio of the inner melt increased. Meanwhile, more inner melt could be pushed and displaced by the water, causing a decrease in the flow resistance of the inner melt. Therefore the penetration area of the water increased.

Moreover, it can be found from Figures 8–11 that although the processing parameters changed, the penetration ratios of the inner melt and the water still decreased with decreasing circle ratio.

CONCLUSIONS

An experimental study of the penetration interfaces in the O-WACIM process of cavities with different cross-sections was carried out based on a lab-developed WACIM system. The influences of the shape of the cavity cross section and the processing parameters on the penetrations of the inner melt and the water were explored. The following conclusions can be drawn.

1. The shape of the penetration section of the inner melt tended to be close to that of the cavity cross-section with round corners, while the shape of the water penetration ended up being round.
2. Both the penetration ratios of the inner melt and the water increased proportionally with increasing circle ratio.
3. The RWT of the skin layer and that of the inner melt were rather even for the circular cross-section cavity. For the non-circular cross-section cavities, both the maximum total RWT and the inner melt RWT occurred at the distal wall and increased nearly proportionally with increasing Max_D, which is the maximum distance between the inscribed circle center and the wall. Both the minimum total RWT and the inner melt RWT increased with increasing circle ratio.
4. Both the penetration ratios of the inner melt and the water increased with increasing water pressure and decreased with increasing water delay time. Both the penetration ratios of the inner melt and the water increased with increasing inner melt flow rate and increasing inner melt temperature.

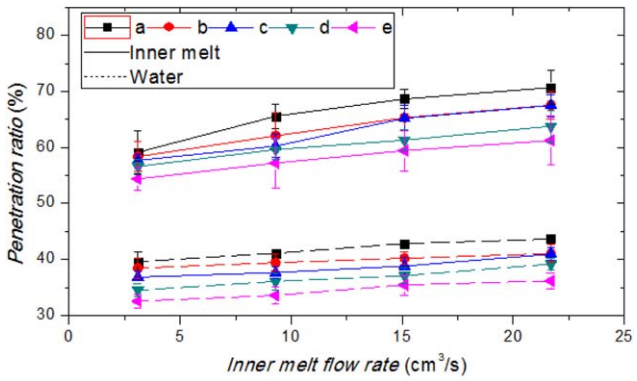

Figure 10. Penetration ratio as a function of inner melt flow rate. (a-e are the no. of the cross-sections). [Color figure can be viewed in the online issue, which is available at wileyonlinelibrary.com.]

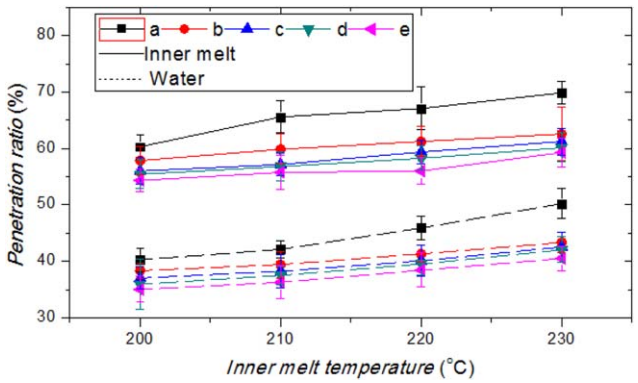

Figure 11. Penetration ratio as a function of inner melt temperature. (a-e are the no. of the cross-sections). [Color figure can be viewed in the online issue, which is available at wileyonlinelibrary.com.]

In order to improve the capability of the O-WACIM process to produce pipes with non-circular cross-sections, a solid projectile will be introduced in this process (converting the process into a water-projectile assisted co-injection molding process) in our future work.

ACKNOWLEDGMENTS

This study was supported by the National Natural Science Foundation of China (NSFC, No. 51103037) for which the authors are very grateful. This project was also supported by the China Scholarship Council (CSC, 2013), the Science and Technology Association of Jiangxi Province (2014), the Wisconsin Institute for Discovery (WID) at the University of Wisconsin–Madison, and the Opening Project of Technology Development Center for Polymer Processing Engineering of Guangdong Province (201501).

REFERENCES

1. Naitove, M. H. *Plastics Technology* **2004**, *50*, 40.
2. Lang, S.; Parkinson, M. J. *Plastics Rubber Compos.* **2005**, *34*, 232.
3. Polynkin, A.; Bai, L.; Pittman, J. F. T.; Sienz, J.; Mulvaney-Johnson, L.; Brown, E.; Dawson, A.; Coates, P.; Brookshaw, B.; Vinning, K.; Butler, J. *Plastics Rubber Compos.* **2008**, *37*, 131.
4. Liu, S. J.; Chen, Y. S. *Compos. A: Appl. Sci. Manuf.* **2004**, *35*, 171.
5. Patcharaphun, S.; Mennig, G. *Polym. Compos.* **2005**, *26*, 823.
6. Zhang, K.; Kuang, T. Q.; Liu, H. S.; Zeng, X. S. *Polym. Mater. Sci. Eng.* **2013**, *29*, 176.
7. Zhang, K.; Liu, H. S.; Kuang, T. Q.; Zeng, X. S. *Polym. Mater. Sci. Eng.* **2013**, *29*, 173.
8. Zhang, K.; Kuang, T. Q.; Liu, H. S.; Zeng, X. S. *China Plast. Ind.* **2013**, *41*, 37.
9. Kuang, T. Q.; Deng, Y. *China Plast.* **2013**, *27*, 105.
10. Yan, L. The Numerical Simulation on Water-Assisted Co-Injection Molding Process. Master's thesis, Nangchang University, Nanchang Jiangxi China, **2007**.

11. Cao, F. C. The Numerical Simulation and Experimental Study on Water-Assisted Co-Injection Molding of Polymer. Master's thesis, Nangchang University, Nanchang Jiangxi China, **2014**.
12. Zhou, G. F.; Cao, F. C.; Zhang, Y. *Eng. Plast. Appl.* **2013**, *41*, 47.
13. Zhou, H.; Chen, Y. L.; Zhang, Z. M.; He, J. J. *J. Mech. Eng.* **2010**, *46*, 170.
14. Kuang, T. Q.; Yu, C. C.; Deng, Y. *CIESC J.* **2014**, *65*, 4176.
15. Kuang, T. Q.; Yu, C. C.; Deng, Y.; Zhou, K.; Turng, L. S. ANTEC2015. Orlando, FL, **2015**, 1766–1770.
16. Selden, R. *Polym. Eng. Sci.* **2000**, *40*, 1165.
17. Li, C. T.; Lee, D. J.; Isayev, A. I. *J. Appl. Polym. Sci.* **2003**, *88*, 2310.
18. Deng, Y. Numerical Simulation and Experimental Study on Water-Assisted Co-Injection Molding Process. Master's thesis, East China Jiaotong University, Nanchang Jiangxi, China, **2014**.
19. Kuang, T. Q.; Yu, C. C.; Deng, Y.; Huang, S. H. *Polym. Mater. Sci. Eng.* **2014**, *30*, 112.
20. Kuang, T. Q.; Deng, Y.; Yu, C. C.; Zhang, K. *Polym. Mater. Sci. Eng.* **2015**, *31*, 121.
21. Huang, H. X.; Deng, Z. W. *J. Appl. Polym. Sci.* **2008**, *108*, 228.
22. Liu, S. J.; Chen, Y. S. *Polym. Eng. Sci.* **2003**, *43*, 1806.
23. Liu, S. J. *Int. Polym. Proc.* **2013**, *24*, 315.
24. Sannen, S.; Keyzer, J. D.; Puyvelde, P. V. *Int. Polym. Proc.* **2013**, *26*, 551.
25. Kuang, T. Q.; Deng, Y. *China Plast.* **2014**, *28*, 96.